Appendix A
Further Exemplary Machine Type Models

A.1 Hard Chrome Plating Model

Hard chrome plating is an electroplating process belonging to the class of coating manufacturing processes. During the process, metallic chrome is electrolytically deposited from an aqueous solution, the electrolyte, by applying electrical energy. As a result, a thin chrome coating emerges on the part while dissolving the electrolyte (Hofmann and Spindler 2014).[1] Figure A.1 shows the general steps of the hard chrome plating process emphasizing those steps which are of high importance for this work with a ■.

Prior to the actual hard chrome plating it is required to use heat treatment to eliminate hydrogen and further gases from the material structure to increase the fatigue strength of the parts. Subsequent to the heat treatment a mechanical pretreatment via grinding or polishing is performed to achieve the defined surface roughness and size accuracy. As a result of the pretreatment the parts require a cleaning from cutting fluid, oil and chip remnants. Due to quality reasons the cleaning is realized using electrolytic degreasing and after that rinsing (Lausmann and Unruh 2006), as illustrated in Figure A.1. To increase the adhesive strength of the chrome coating, the part is further anodically etched.[2] Subsequent to the actual hard chrome plating process, the parts are rinsed again and dried to remove potentially remaining electrolyte before they are mechanically finished via polishing or grinding processes.

[1] Typical thicknesses of hard chrome plating layers start at $\geq 2\,\mu m$ usually ranging up to $100\,\mu m$. Chrome plating layers are marked by high hardness (800–1100 HV) and wear resistance, low coefficient of friction as well as good corrosion and heat resistance (until 400 °C) (Weiner 1974; Kanani 2005). Because of these layer properties hard chrome plating is for example often applied to hydraulic parts.

[2] This process is often also referred to as 'activated'. Since chromic acid based electrolytes are usually acidic they exhibit a high oxidation potential immediately triggering an acid corrosion as well as the formation of a passivation layer on the part. Because the passive layer always has a share of chromium oxide this step ensures the electrical conductivity of the part (Lausmann and Unruh 2006).

D. Kurle, *Integrated Planning of Heat Flows in Production Systems*,
Sustainable Production, Life Cycle Engineering and Management,
https://doi.org/10.1007/978-3-319-70440-1

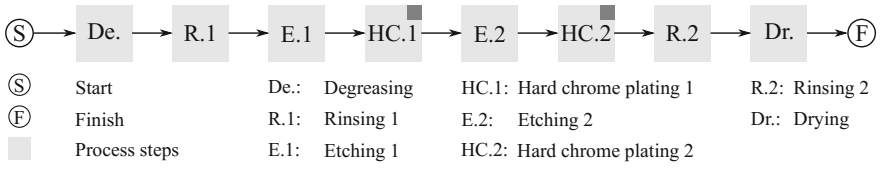

Fig. A.1 General hard chrome plating steps

Hard chrome plating ■ represents the major process steps which is why they are explained in more detail. Subsequent to the etching, the part is immersed into the process bath and used as a cathode. As a consequence, the outside of the passive layer provides electrons for reduction procedures initiating the deposition of the chrome from the electrolyte onto the part unless the critical current density[3] is retained.

Besides the actual metal deposition ($Cr^{6+} \rightarrow Cr^0$) further secondary reactions such as the reduction of chrome ($Cr^{6+} \rightarrow Cr^{3+}$) and hydrogen separation ($2H^+ + 2e^- \rightarrow H_2$) take place during the electrolysis. This entails that only limited shares of the induced electrical current can be used for the electrochemical deposition leading to a higher required charge quantity R than analytically calculated for example by using the law of Faraday.[4]

To take this aspect into account another term known as the electricity yield (EY) describes the relation between the employed charge quantity R_{em} and the total charge quantity R_{tot} (Lausmann and Unruh 2006):

$$EY = \frac{R_{em}}{R_{tot}} \cdot 100\%, \quad \text{with} \quad R = \int_{t_0}^{t} I \, \mathrm{d}t. \tag{A.1}$$

In addition to that, the employed electrolyte has also an impact on the EY of the hard chrome plating process.[5] Chrome electrolytes comprise besides water, chrome acid or rather Cr_2O_3 (concentration $\beta = 180$–350 g/l) and catalysts.[6] Depending on the

[3]Below the critical current density only chrome(III)bonds and hydrogen are formed and no chrome is electrolytically deposited yet. The critical current density further depends on the chrome and external acid content as well as the material of the part. More details about the process of separating chrome, which has not been fully understood up to-date, can be found in Lausmann and Unruh (2006) and Distelrath-Lübeck (2012).

[4]Pursuant to the law of Faraday metal deposition describes a mass transfer of the mass m_F, which is initiated by the charge quantity R between the electrode and the electrolyte which can be written as: $m_F = E_e \cdot R$, where E_e is referred to as the electrochemical equivalent stating the quality of the process (Unruh 2001).

[5]Electrolytes for hard chrome plating processes usually base on chrome(VI) bonds (Distelrath-Lübeck 2012).

[6]Typical catalysts such as sulphate ions (concentration of 1.8–6 g/l) or fluoride ions ($< 2\%$ of chrome acid concentration) ensure that chrome ions are dissolved out of their hydrate shell and to be discharged to initiate the chrome separation (Hofmann and Spindler 2014; Umweltbundesamt 2005). Furthermore, fluorine tenside in the electrolyte decrease the surface tension leading to fewer carry-over losses and reduced spray bath fog (Lausmann and Unruh 2006).

Table A.1 Parameter correlations of the hard chrome process; own representation based on Lausmann and Unruh (2006)

Change of parameter		Effect
(i)	Temperature T ↑	Hardness ↓, Throwing power ↓
(ii)	Content of foreign ions ↑ (due to high catalyst content)	Throwing power ↓
(iii)	Concentration of chrome acid β	Throwing power ↑
(iv)	Temperature T ↑	EY ↓ (drastic decrease above T = 56 °C)
(v)	Current density ↑	EY ↑
(vi)	EY = f(β) EY depends on the β and the share of foreign ions due to catalysts as well as the relation between chrome acid and foreign ions	

choice of catalyst the final chrome surface can be influenced in terms of look, physical (cracking) as well as chemical and mechanical properties (wear and corrosion resistance) (Distelrath-Lübeck 2012; Umweltbundesamt 2005). Although catalysts may improve certain process characteristics, its content must not be too high because it entails a strong etching of non-chromed surfaces leading to a significant increase in foreign ions in the electrolyte. This again impedes the electrolytes throwing power describing the capability to achieve an uniform layer structure.

Thus, the composition of the electrolyte and its ingredients as well as resulting impurities may entail a strong influence on physical process indicators such as the EY and the throwing power (Lausmann and Unruh 2006). As a consequence, it is important to continuously monitor the impurity content of the hard chrome plating bath as well as the main process parameters which is often only based on empirical data instead of analytic relations.

Table A.1 shows derived fundamental correlations of parameters for the hard chrome plating process.

With respect to Table A.1, particularly the parameters temperature T, current density J and concentration of chrome acid β seem to exhibit a high impact on the EY. Because of that, Figure A.2 shows the EY for an electrolyte with sulfate ions as a catalyst subject to the concentration of chrome acid β with $J = 20\,\mathrm{A/dm^2}$ and $T = 56\,^{\circ}\mathrm{C}$. As a result, it can be seen that the functional correlation between EY and β is non-linear similar to a downwardly opened parabola (Lausmann and Unruh 2006). Due to the high relevance of this parameter it is important to monitor this parameter closely.

Abstraction and Modeling

Machine States

Figure A.3 shows the associated process step logic in form of different state charts and involved DES simulation modeling elements. Since hard chrome plating processes often represent batch processes involving multiple products which move from process step to process step, various activating and deactivated conditions for each

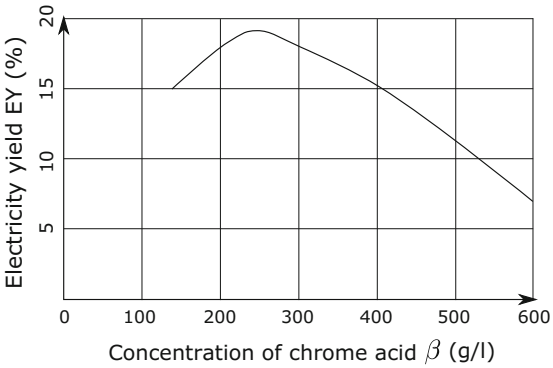

Fig. A.2 Functional correlation between the electricity yield and the concentration of chrome acid (Lausmann and Unruh 2006)

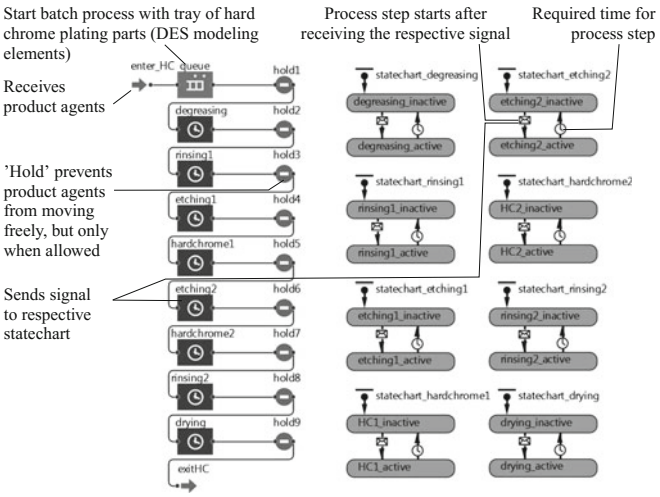

Fig. A.3 State chart showing the process step logic of the hard chrome plating model

process step are included. The reason for using multiple state charts is based on the modeling advantages resulting from a decoupling of process steps from each other. This facilitates the modeling to route batches from process step to process step.

To steer the individual activating and deactivating of the respective process steps, the hard chrome plating model uses different DE modeling elements. Those elements receive as opposed to for instance the machining model not only a starting signal from the higher system level (which is the generic machine model in this case), but entire product agents. Those agents first enter the hard chrome plating model and wait in a *queue element* which is closed by a *hold element* in case not all product agents for a certain batch size have arrived at the machine yet. As soon as this condition is sufficed either a single product agent or a batch involving multiple

product agents is routed to the first process step *degreasing* indicated by a *delay element*. Upon entering the respective process step a signal is sent to the respective state charts *startchart_degreading*. This signal triggers a change in condition per process step by activating it (as shown in Figure A.3 for the process step *etching2*). After the processing time the product agent (batch) leaves the process step unless the subsequent process step is available yet. Otherwise the product agent (batch) remains and therefore blocks the current process step. This procedure iterates for all involved process steps.

Heat Flows

Subsequent to the description of the process steps, its modeled states and therefore the physical setup of the hard chrome plating process, this paragraph further details the actual hard chrome plating baths from the general hard chrome plating steps shown in Figure A.1. In that regard, seven relevant heat flows are identified. Each heat flow is allotted to one of five different types of heat flow as explained below.

(i) substance-related:	through evaporation (E) (↟1)
(ii) through radiation:	on the electrolyte surface (↟2)
(iii) through convection:	to the hard chrome plated WP (↟3)
	to the exhaust air and FA (↟4)
(iv) through heat conduction:	to the CW (↟5)
	to the walls of the bath or MC (↟6)
(v) conversion losses:	degree of efficiency of rectifier (↟7)

Figure A.4 further shows the seven different heat flows pursuant to Table's 4.9 notation. Since the electrolyte requires a certain temperature range to work properly, it is important to maintain a constant operating temperature of the hard chrome bath. Because of the process relevant induced electrical energy the electrolyte is prone to heat up. Thus, the heat balance of the process needs to be regulated carefully despite having present different heat flows (↟1–5) coming from the hard chrome bath. A heat exchanger in the electrolyte circulation system ensures a cooling of the electrolyte. The emergence of toxic aerosols (Umweltbundesamt 2005) during the process demands the existence of an exhaust air system resulting in heat flow (↟6). The electrical process energy comes from a rectifier with a degree of efficiency leading to a heat flow due to conversion losses (↟7). The calculation of heat flow (↟7) follows Eq. 4.8. However, since Sect. 4.4.1.2 already describes the general heat transfer mechanisms occurring during a machining process in detail, this section focuses on heat flows that are of particular relevance for the hard chrome plating process, namely heat flow (↟ 1) and (↟ 5).

Heat Flow (↟ 1) *Through Evaporation*

To calculate heat flow (↟ 1) as a result from evaporation losses it is necessary to determine the amount of evaporation. This can be realized in two different ways either based on empirical data and possibly interpolation or by using an equation.

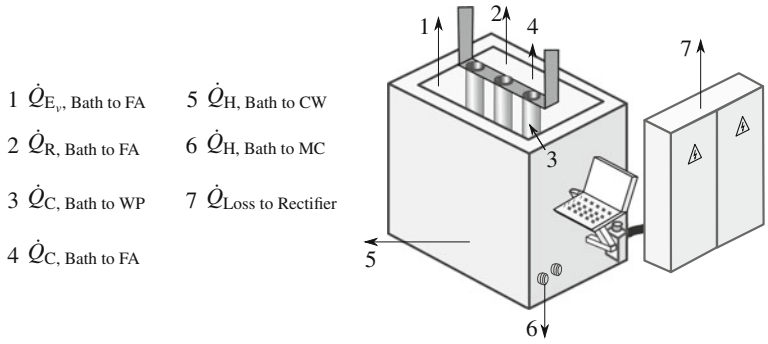

Fig. A.4 Schematic representation of a hard chrome plating bath with heat flows; abbreviations used: machine case (MC), cooling water (CW), factory air (FA)

The determination based on empirical data states the amount of evaporation subject to specific values for the electrolyte temperature and the air velocity. Case specific values can be computed by interpolating between the given empirical values.[7] An equation based option to compute the amount of evaporation per hour and square meter geared to the needs of the hard chrome plating process reads as follows (Giebler and Knechtel 2009b):

$$E_v\left(T_{electr.}, v, \varphi, T_{air}\right) = p_0 \left[e^{\left(\frac{c_1 \cdot T_{electr.}}{c_2 + T_{electr.}}\right)} - \varphi \cdot e^{\left(\frac{c_1 \cdot T_{air}}{c_2 + * T_{air}}\right)} \right] \cdot \frac{k_1 + k_2 \cdot v_{air}^{\xi}}{\kappa_1 + \kappa_2 \cdot T_{air}} \cdot K_E \quad \text{(A.2)}$$

With respect to Eq. A.2 it can be seen that the computed amount of evaporation depends on the temperature of the electrolyte $T_{electr.}$, the air velocity v, the air temperature T_{air} and the relative humidity φ of the surrounding air. Furthermore, an adjustment factor K_E is introduced to consider substantial influences on the amount of evaporation caused by different electrolytes.

However, a comparison of both methods reveals discrepancies regarding the amount of evaluation, as shown in Table A.2.

In general both calculation methods can be employed, but for the developed model only the method based on empirical data using interpolation to ensure more flexibility is employed.

[7] A specific data table can be found in Unruh (2001) on page 561.

Table A.2 Comparison of methods for determining the amount of evaporation

Value based on empirical data	Value based on Eq. A.2	Unit
0.00138111	0.00248324	[kg/s]

Heat Flow (↟ 5) Through Cooling Water

To accurately compute the dissipated process heat being removed by the cooling system, it is important to understand which factors may influence the bath internal emergence of process heat. In that context, the EY states such an important factor due to its correlation to the temperature, as indicated in Table A.1. In addition to that, EY is dependent on the β which cannot be formalized yet and is therefore modeled and expressed by an empirically derived regression function. Figure A.5 shows three regression functions for its respective electrolyte (H2SiF6, HF, H2SO4) which have been chosen and modeled due to its common usage.

The same situation applies for the deposition rate $v_{process}$ as a function of the empirically determined EY and the current density J. Figure A.6 illustrates this relation based on interpolated integer values from Lausmann and Unruh (2006)[8] indicating that $v_{process}$ increases with rising values for EY and J.

This again directly influences the process time as a ratio of the layer thickness and $v_{process}$. As a result, the model continuously updates the mutual relationships implying that a decreasing concentration of chrome acid β and thus a reducing EY and $v_{process}$ entails a longer process time $t_{process}$. The process time again has an influence on the total charge quantity according to Eq. A.1.

$$R_{tot} = I \cdot \frac{t_{process}}{60\frac{min}{h}} \tag{A.3}$$

By employing the enthalpy of formation of the used substances on the hard chrome plating process, the resulting heat can be further quantified. This is exemplarily shown

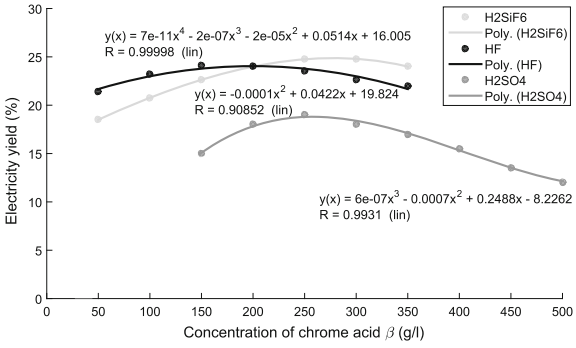

Fig. A.5 Empirical approximation of the correlation between EY and β for three different electrolytes; own representation with data from Lausmann and Unruh (2006)

[8]The data can be found on page 513.

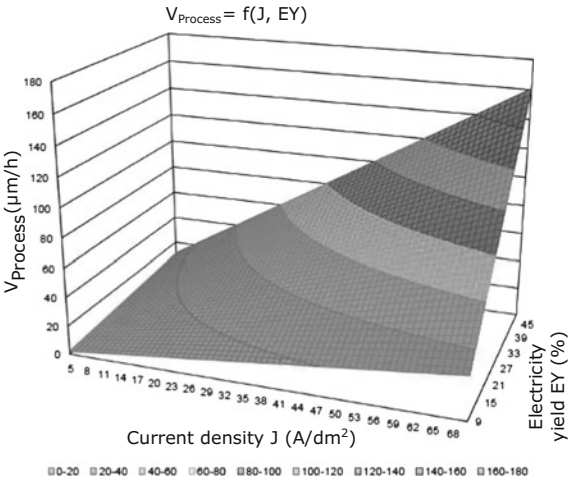

Fig. A.6 Empirical approximation of the deposition rate $v_{process}$ as a function of the current density J and EY interpolated with values from Lausmann and Unruh (2006)

in a simplified manner[9] for the chrome and hydrogen deposition. The gross reaction of the chrome and hydrogen deposition yields:

$$\underbrace{2Cr_2O_7^{2-} + 14H^+ + 12e^- \rightarrow 2Cr + 7H_2O}_{Chrome} \quad , \quad \underbrace{2H_3O^+ + e^- \rightarrow H_2 + 2H_2O}_{Hydrogen} . \tag{A.4}$$

By using further the molecular mass and the net formation enthalpy of chrome and hydrogen, as shown in Table A.3, the following equations provide a way for approximating the required amount of heat to be removed by the cooling system.

The employed charge quantity of chrome and hydrogen can be calculated pursuant to Eq. A.1 as follows:

$$R_{chrome} = EY \cdot R_{tot} \qquad R_{hydrogen} = (1 - EY) \cdot R_{tot} \tag{A.5}$$

taking into account the amount of substance employed:

$$n_{chrome} = \frac{R_{chrome} \cdot E_e^{chrome}}{M_{chrome}} \qquad n_{hydrogen} = \frac{R_{hydrogen} \cdot E_e^{hydrogen}}{M_{hydrogen}} \tag{A.6}$$

as well as the required energy for it:

$$E_{chrome} = \Delta H_f^{chrome} \cdot n_{chrome} \qquad E_{hydrogen} = \Delta H_f^{hydrogen} \cdot n_{hydrogen}. \tag{A.7}$$

Assuming the rectifier provides the hard chrome plating bath with an energy $E_{rectifier}$, the resulting process heat amounts to that subtracted by E_{chrome} and

[9] Assuming only dichromates exist in the electrolyte triggering the deposition.

Table A.3 Chrome and hydrogen parameters

Parameter	Symbol	Value
Net formation enthalpy of chrome	ΔH_f^{chrome}	489 kJ/mol
Net formation enthalpy of hydrogen	$\Delta H_f^{hydrogen}$	286 kJ/mol
Molecular mass of chrome	M^{chrome}	52 g/mol
Molecular mass of hydrogen	$M^{hydrogen}$	2 g/mol

$E_{hydrogen}$. The result of this difference reduced by the heat flows (↟ 1)–(↟ 4) and (↟ 6) from Figure A.4 yields the process heat to be removed by the cooling system.

Implementation

The hard chrome plating model is also implemented as an individual machine type of a hard chrome plating agent class. Each respective agent affiliates to one generic machine model agent and comprises diverse state charts and DE modeling elements from the Anylogic™ process modeling library (as shown in Figure A.3). Furthermore, the class contains several parameters, static as well as dynamic variables and functions computing the aforementioned relations and heat flows. To reflect the continuous behavior of heat flows, dynamic system elements are used to imitate the underlying differential equations. Different diagrams plot the resulting heat flows and help comparing and visualizing their respective magnitude and behavior.

Besides the dynamic heat flow calculations, the functions and variables further ensure stable process conditions for instance by adjusting the amount of electrolyte to be refilled to guarantee a sufficiently high concentration of β subject to for example evaporation and carryover of electrolyte.

The specification of empirically determined data via interpolation is outsourced to MS Excel where all empirical data sets are stored. This saves memory for the simulation and facilitates a direct alteration of data. Those parameters as well as all other user specified parameters are then loaded by the simulation.

The hard chrome plating model presents an empirically modeled machine type model. It is based on measured data and derived functional relationships as opposed to mainly analytic relations. It further shows how unknown heat flows can be deduced from process knowledge.

A.2 Die Casting Machine Model

Die casting processes generally use either hot and cold chamber die casting machines. This work focuses on cold die casting machines due to its broader field of application regarding the casting material.[10] Figure A.7 illustrates the major steps of the die casting process highlighting the heat relevant process steps with a ■. In that regard particular interest is put on the emerging heat of smelting and cooling processes and its repercussions on involved machine elements such as the form.

Preheat form ■ After closing the form, a temperature control ensures a preheating of the form via several heating channels for a thermal transfer fluid (Nogowizin 2011). This is necessary due to several quality reasons.[11] From an efficient production perspective, this process step is intended to be performed quickly to avoid unproductive machine times. However, this entails that a significant amount of heat needs be transferred to the massive forms in a very short period of time. In that regard, the initial preheating of the forms takes up the major share of induced electricity of the temperature control. Whereas the subsequent running the temperature control requires significantly less power.

Smelting ■ The actual smelting of the casting material[12] takes place in a separate oven where it is heated up to the liquidus. Typically employed alloys often do not have a fixed solidification point but rather an interval varying between the solidus (T_S) and a liquidus temperature (T_L). Within this interval the melt contains solid as well as liquid elements. Figure A.8 visualizes this interval as well as foregoing and following intervals[13].

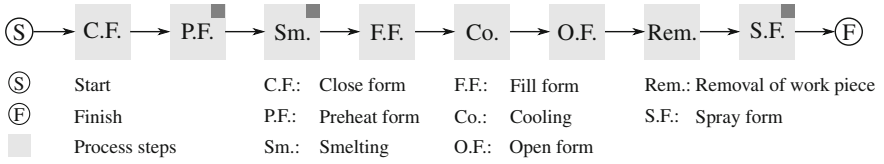

Fig. A.7 General die casting steps (inspired by Heinrich 2003)

[10] Hot chamber die casting machines usually include the shot assembly inside the machine and the process itself is limited to specific casting materials, preferably with a low melting temperature such as zinc. Fritz and Schulze (2010) and Brunhuber (1980) provide more information on this process.

[11] The preheating of the forms prevent thermally induced internal stresses from occurring. Furthermore, it impedes local solidification of the part (Nogowizin 2011).

[12] Typical casting materials comprise aluminum including alloying elements such as magnesium, copper or silicon (Nogowizin 2011).

[13] In interval (I) the work piece receives heat until ϑ_S is reached. The melting occurs in interval (II). The rise in this interval is subject to the greater specific heat of fusion h_a in a relatively small temperature interval compared with the specific heat capacity c_p. Although c_p increases with the temperature, h_a exceeds c_p by several orders of magnitude leading to a flatter gradient in interval (II) of Figure A.8 (Nogowizin 2011).

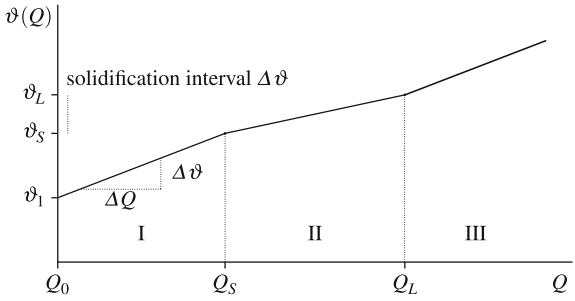

Fig. A.8 ϑ-Q diagram of a work piece with a cooling interval between solidus ϑ_S and liquidus temperature ϑ_L

Thus, three different areas described by the function $\vartheta(Q)$ follow that need to be taken into account when modeling the cooling and melting behavior. Both the cooling and melting behavior can be described alike by:

$$\vartheta(Q) = \begin{cases} \vartheta_1 + \frac{1}{m \cdot c_p} \cdot (Q - Q_0) & \text{with } 0 \leq Q < Q_S \text{ (I)} \\ \vartheta_S + \frac{\vartheta_L - \vartheta_S}{m \cdot (h_a + c_p)} \cdot (Q - Q_S) & \text{with } Q_S \leq Q < Q_L \text{ (II)} \\ \vartheta_L + \frac{1}{m \cdot c_p} \cdot (Q - Q_L) & \text{with } Q_L \leq Q \text{ (III).} \end{cases} \tag{A.8}$$

When computing the added heat for the die casting process, an exemplary melting from the room temperature (ϑ_1) to the liquidus temperature (ϑ_L) can be expressed by (this can also be used for the process step cooling[14]

$$Q_{\mathrm{L1}} = \underbrace{V \cdot \rho_L \cdot \left(h_a + c_a \cdot (\vartheta_L - \vartheta_S)\right)}_{Q_{LS}\,(II)} + \underbrace{V \cdot \rho_L \cdot \left(c_m \cdot (\vartheta_S - \vartheta_1)\right)}_{Q_{S1}\,(I)} \tag{A.9}$$

using the following terms: volume inside the forms (V), density of the alloy at T_L (ρ_L), specific heat of fusion or cooling of the alloy (h_a), mean specific heat capacity of the alloy in a semi-liquid state (c_a) and mean specific heat capacity of the alloy at the mean temperature (between T_1 and T_S) (c_m).

In case the required casting temperature ϑ_C exceeds ϑ_L the superheat can be estimated by:

$$Q_{\mathrm{CL}} = \underbrace{V \cdot \rho_L \cdot c_a \cdot (\vartheta_C - \vartheta_L)}_{Q_{CL}\,(III)} \tag{A.10}$$

Spray form ■ This step helps to remove all residues from the process via compressed air and cools the form by spraying water and a cast separating agent on it (Nogowizin

[14] During the cooling heat is transferred to the form until the cast reaches the demolding temperature ϑ_D. As a result the temperature of the form increases particularly at the contact areas between the form and the cast. The outer temperature of the form can be approximated by: $\vartheta_{F_{outside}} = \vartheta_{air} + 0.6 \cdot \left(\vartheta_{F_{inside}} - \vartheta_{air}\right)$ (Nogowizin 2011) and used to determine the other heat flows from the form to the factory air ($\dot{Q}_{\mathrm{C,\ Form\ to\ FA}}$), to the walls ($\dot{Q}_{\mathrm{R,\ Form\ to\ FW}}$) and the form holding elements ($\dot{Q}_{\mathrm{H,\ Form\ to\ Clamps}}$).

2011). However, the model assumes that this process step is realized by only using water which is completely evaporated[15, 16].

A.3 Heat Treatment Model

Heat treatment states a heat and waste heat relevant process and adds to the aforementioned modeling aspects the influence of different material structures and its respective process parameters.

Heat treatment comprises many different process types either used to put work pieces in an intermediate state to improve processing properties or a final state (Tinscher and Zoch 2015b). This work regards precipitation hardening as a heat treatment process to increase the strength of non-ferrous materials (Keßler 2015). Figure A.9 depicts the general process steps emphasizing the heat relevant steps with a ■.

These three steps are further qualitatively visualized in Figure A.10 showing the temporal temperature profile.

Since from a modeling logic perspective the three heat relevant steps can be modeled quite similar, the following remarks therefore only focus on the first process step (solution annealing).

Solution annealing ■ During this process step it is intended to achieve a homogeneous formation of for example α_{Al}-mixed crystals. This is realized through diffusion processes fostering the subsequent material hardening (Kammer 2012). To achieve this, particularly two different parameters require careful fine tuning, the *annealing temperature* ($\vartheta_{S.A}$) and the *annealing time* ($t_{S.A}$).[17] Regarding $\vartheta_{S.A}$ it is important to choose a high value just below the melting temperature to achieve a short $t_{S.A}$ describing the required time to reach $\vartheta_{S.A}$.[18] Similar aspects for the temperature and

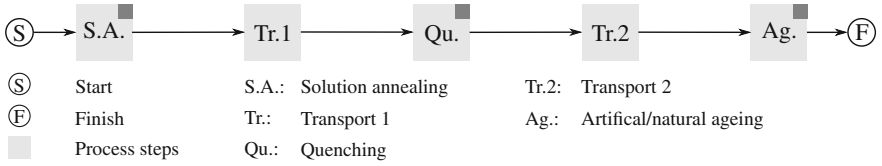

Fig. A.9 General precipitation hardening steps

[15] Typical values for the heat transfer coefficients for the spraying come from Chabičovský and Raudenský (2013).

[16] A comprehensive description and exemplary calculation of all heat relevant flows can be found in Röders et al. (2006).

[17] This general correlation also applies for the other two relevant process steps from Figure A.10 (quenching and artificial/natural ageing).

[18] $t_{S.A}$ also depends on the geometrical structure of the work piece as well as the distribution of alloy elements (Keßler 2015).

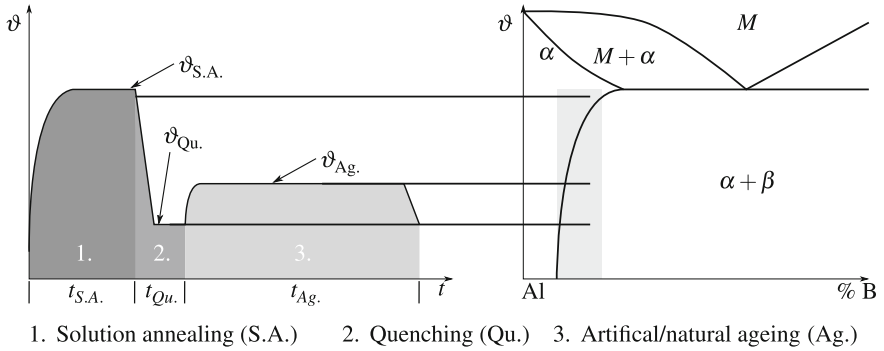

Fig. A.10 Temporal temperature profile during precipitation hardening and its corresponding phase diagram, in reference to Kammer (2012)

time also apply for the process steps quenching and artificial/natural ageing at their respective temperature and time levels which will not be further at this point due to possibly redundant explanations.[19] The previously explained correlations between heat flows in Sect. 4.4.1.2 generally apply for this process as well.

References

1. Hofmann H, Spindler J (2014) Verfahren in der Beschichtungs- und Oberflchentechnik. Hanser, 3., überarb. aufl. edition
2. Weiner R (1974) Die galvanische Verchromung. Leitfaden fr die moderne Glanz- und Hartverchromung, volume 2. of Schriftenreihe Galvanotechnik, 6. Eugen G.Leutze Verlag
3. Kanani N (2005) Electroplating. Basic principles, processes and practice. Elsevier, 1. aufl. edition. http://gbv.eblib.com/patron/FullRecord.aspx?p=316911
4. Lausmann GA, Unruh J (2006) Die galvanische Verchromung. Mit 66 Tabellen. Schriftenreihe Galvanotechnik und Oberflchenbehandlung, 35. Leuze, 2., komplett berarb. aufl. edition. ISBN 978-3-410-22028-2
5. Distelrath-Lübeck A (2012) Untersuchungen zum Mechanismus der Abscheidung strukturierter Schichten aus sechswertigen Chrom-Elektrolyten. PhD thesis. https://www.db-thueringen.de/receive/dbt_mods_00020980
6. Unruh JN (2001) Tabellenbuch Galvanotechnik. Leuze, 7. aufl. edition
7. Umweltbundesamt (2005) Integrierte Vermeidung und Verminderung der Umweltverschmutzung - Merkblatt zu den besten verfgbaren Techniken fr die Oberflächenbehandlung von Metallen und Kunststoffen. https://www.umweltbundesamt.de/sites/default/files/medien/419/dokumente/bvt_galvanik_vv.pdf
8. Giebler E, Knechtel A (2009b) Abhängigkeit der Verdunstung aus galvanotechnischen Prozess- und Spüllösungen (Fortsetzung). Galvanotechnik 11:2856–2869
9. Fritz A-H, Schulze G (2010) Fertigungstechnik
10. Brunhuber E (1980) Praxis der Druckgußfertigung. Schiele & Schön, 3., neubearbeitete und erweiterte auflage edition. ISBN 3-7949-0342-0

[19] Further information about the process can be found in Specht (2014).

11. Heinrich F (2003) Leichtbauverbundstrukturen durch Umgießen von Aluminiumschaumkernen im Druckguss. https://opus4.kobv.de/opus4-fau/frontdoor/index/index/docId/38
12. Nogowizin B (2011) Theorie und Praxis des Druckgusses. Schiele & Schön. ISBN 978-3-7949-0796-0
13. Chabičovský M, Raudenský M (2013) Experimental investigation of spray cooling of horizontally and vertically oriented surfaces. In: TANGER Ltd., editor, Metal 2013, pp 198–203
14. Röders G, Indorf C, Dilger K, Pries H, Anders U (2006) Optimierung der Energiebilanz beim Aluminium-Druckguss. https://www.dbu.de/OPAC/ab/DBU-Abschlussbericht-AZ-22197.pdf
15. Tinscher R, Zoch H-W (2015) Grundlagen der Wärmebehandlung. In: Zoch H-W, Spur G (eds) Handbuch Wärmebehandeln und Beschichten, Handbuch der Fertigungstechnik, pp 263–303. Carl Hanser Verlag. ISBN 978-3-446-42779-2
16. Keßler O (2015) Wärmebehandlung von Nichteisenmetalllegierungen. In Zoch H-W, Spur G (eds) Handbuch Wärmebehandeln und Beschichten, Handbuch der Fertigungstechnik, pp 555–580. Carl Hanser Verlag. ISBN 978-3-446-42779-2
17. Kammer C (2012) Aluminium-Taschenbuch 1. Beuth, 16. edition. ISBN 978-3-410-22028-2
18. Specht E (2014) Intensivkühlung heißer Metalle mit Flüssigkeiten. In Grote K-H, Feldhusen J (eds) Dubbel. Springer, Berlin, pp P75–P87. ISBN 978-3-642-38890-3. https://doi.org/10.1007/978-3-642-38891-0_71

Appendix B
Data Tables for the Cooling Tower(s) Model

B.1 Material Values of Saturated Air

(See Table B.1)

Table B.1 Material values of saturated air

T (°C)	p_S (mbar)	x_S (kg/kg)	h_S (kJ/kg)	ρ_A (kg/m^3)	T (°C)	p_S (mbar)	x_S (kg/kg)	h_S (kJ/kg)	ρ_A (kg/m^3)
–20	1.029	0.64	–18.534	1.38	20	23.37	14.88	57.882	1.18
–19	1.133	0.71	–17.366	1.37	21	24.85	15.85	61.369	1.17
–18	1.246	0.78	–16.187	1.37	22	26.42	16.88	65.019	1.17
–17	1.369	0.85	–14.99	1.36	23	28.08	17.97	68.831	1.16
–16	1.503	0.94	–13.778	1.35	24	29.82	19.12	72.791	1.16
–15	1.649	1.03	–12.543	1.35	25	31.67	20.34	76.937	1.16
–14	1.808	1.13	–11.29	1.34	26	33.6	21.63	81.266	1.15
–13	1.98	1.23	–10.018	1.34	27	35.64	22.99	85.785	1.15
–12	2.169	1.35	–8.717	1.33	28	37.78	24.42	90.496	1.14
–11	2.373	1.48	–7.395	1.33	29	40.04	25.94	95.434	1.14
–10	2.595	1.62	–6.041	1.32	30	42.41	27.52	100.517	1.13
–9	2.833	1.77	–4.663	1.32	31	44.91	29.25	105.996	1.13
–8	3.095	1.93	–3.247	1.31	32	47.53	31.07	111.729	1.12
–7	3.376	2.11	–1.799	1.31	33	50.29	32.94	117.567	1.12

(continued)

D. Kurle, *Integrated Planning of Heat Flows in Production Systems*,
Sustainable Production, Life Cycle Engineering and Management,
https://doi.org/10.1007/978-3-319-70440-1

Table B.1 (continued)

T (°C)	p_S (mbar)	x_S (kg/kg)	h_S (kJ/kg)	ρ_A (kg/m^3)	T (°C)	p_S (mbar)	x_S (kg/kg)	h_S (kJ/kg)	ρ_A (kg/m^3)
–6	3.681	2.3	0	1.3	34	53.18	34.94	123.758	1.11
–5	4.011	2.51	1.211	1.3	35	56.22	37.05	130.257	1.11
–4	4.368	2.73	2.78	1.29	36	59.4	39.28	137.053	1.1
–3	4.754	2.97	4.393	1.29	37	62.74	41.64	144.19	1.1
–2	5.172	3.23	6.059	1.28	38	66.24	44.12	151.67	1.09
–1	5.621	3.52	7.778	1.28	39	69.91	46.75	159.52	1.09
0	6.108	3.82	9.555	1.27	40	73.75	49.52	167.732	1.08
1	6.565	4.11	11.289	1.27	41	77.77	52.45	176.39	1.08
2	7.054	4.42	13.074	1.26	42	81.98	55.45	185.469	1.07
3	7.574	4.75	14.91	1.26	43	86.39	58.82	195.022	1.07
4	8.129	5.1	16.804	1.25	44	91	62.26	205.033	1.06
5	8.718	5.47	18.755	1.25	45	95.82	65.92	218.599	1.06
6	9.346	5.87	20.769	1.24	46	100.85	69.76	226.68	1.05
7	10.013	6.29	22.848	1.24	47	106.12	73.84	238.369	1.05
8	11.721	6.74	24.998	1.23	48	111.62	78.15	250.671	1.04
9	11.473	7.22	27.219	1.23	49	117.36	82.7	263.628	1.03
10	12.271	7.73	29.519	1.23	50	123.35	87.52	277.274	1.03
11	13.117	8.27	31.9	1.22	51	129.6	92.61	291.665	1.02
12	14.015	8.84	34.368	1.22	52	136.13	98.01	306.85	1.02
13	14.969	9.45	36.929	1.21	53	142.93	103.73	322.911	1.01
14	15.974	10.1	39.587	1.21	54	150.02	109.78	339.859	1
15	17.04	10.78	42.344	1.2	55	157.41	116.19	357.749	1
16	18.169	11.51	45.212	1.2	56	165.09	122.99	376.687	0.99
17	19.363	12.28	48.168	1.19	57	173.12	130.23	396.785	0.99
18	20.62	13.1	51.281	1.19	58	181.46	137.89	418.02	0.98
19	21.957	13.97	54.493	1.18	59	190.15	146.04	440.571	0.97

B.2 Enthalpy-Dependent Temperatures and Water Loads of Saturated Air

(See Table B.2)

Table B.2 Enthalpy-dependent temperatures and water loads of saturated air

h_S (kJ/kg)	T (°C)	x_S (kg/kg)	h_S (kJ/kg)	T (°C)	x_S (kg/kg)	h_S (kJ/kg)	T (°C)	x_S (kg/kg)
–19	–20	0.641	102	30	27.52	207	44	62.261
–18	–20	0.641	103	30	27.52	208	44	62.261
–17	–19	0.706	104	31	29.247	209	44	62.261
–16	–18	0.776	105	31	29.247	210	44	62.261
–15	–17	0.853	106	31	29.247	211	44	62.261
–14	–16	0.936	107	31	29.247	212	44	62.261
–13	–15	1.028	108	31	29.247	213	45	65.916
–12	–15	1.028	109	31	29.247	214	45	65.916
–11	–14	1.127	110	32	31.073	215	45	65.916
–10	–13	1.234	111	32	31.073	216	45	65.916
–9	–12	1.352	112	32	31.073	217	45	65.916
–8	–12	1.352	113	32	31.073	218	45	65.916
–7	–11	1.479	114	32	31.073	219	45	65.916
–6	–10	1.618	115	32	31.073	220	45	65.916
–5	–9	1.767	116	33	32.937	221	45	65.916
–4	–9	1.767	117	33	32.937	222	45	65.916
–3	–8	1.931	118	33	32.937	223	45	65.916
–2	–7	2.107	119	33	32.937	224	46	69.764
–1	–7	2.107	120	33	32.937	225	46	69.764
0	–6	2.298	121	33	32.937	226	46	69.764
1	–5	2.505	122	34	34.936	227	46	69.764
2	–5	2.505	123	34	34.936	228	46	69.764
3	–4	2.729	124	34	34.936	229	46	69.764
4	–3	2.971	125	34	34.936	230	46	69.764
5	–3	2.971	126	34	34.936	231	46	69.764
6	–2	3.233	127	34	34.936	232	46	69.764
7	–2	3.233	128	35	37.052	233	47	73.843
8	–1	3.516	129	35	37.052	234	47	73.843
9	–1	3.516	130	35	37.052	235	47	73.843
10	0	3.822	131	35	37.052	236	47	73.843
11	1	4.11	132	35	37.052	237	47	73.843
12	1	4.11	133	35	37.052	238	47	73.843
13	2	4.419	134	36	39.28	239	47	73.843
14	2	4.419	135	36	39.28	240	47	73.843
15	3	4.747	136	36	39.28	241	47	73.843
16	3	4.747	137	36	39.28	242	47	73.843
17	4	5.098	138	36	39.28	243	47	73.843

(continued)

Table B.2 (continued)

h_S (kJ/kg)	T ($^\circ C$)	x_S (kg/kg)	h_S (kJ/kg)	T ($^\circ C$)	x_S (kg/kg)	h_S (kJ/kg)	T ($^\circ C$)	x_S (kg/kg)
33	11	8.267	144	37	41.636	249	48	78.151
34	12	8.841	145	37	41.636	250	48	78.151
35	12	8.841	146	37	41.636	251	48	78.151
36	13	9.45	147	37	41.636	252	48	78.151
37	13	9.45	148	37	41.636	253	48	78.151
38	13	9.45	149	38	44.124	254	48	78.151
39	14	10.097	150	38	44.124	255	48	78.151
40	14	10.097	151	38	44.124	256	48	78.151
41	14	10.097	152	38	44.124	257	48	78.151
42	15	10.783	153	38	44.124	258	48	78.151
43	15	10.783	154	38	44.124	259	49	82.704
44	16	11.511	155	38	44.124	260	49	82.704
45	16	11.511	156	38	44.124	261	49	82.704
46	16	11.511	157	39	46.752	262	49	82.704
47	17	12.28	158	39	46.752	263	49	82.704
48	17	12.28	159	39	46.752	264	49	82.704
49	17	12.28	160	39	46.752	265	49	82.704
50	18	13.096	161	39	46.752	266	49	82.704
51	18	13.096	162	39	46.752	267	49	82.704
52	18	13.096	163	39	46.752	268	49	82.704
53	19	13.966	164	39	46.752	269	49	82.704
54	19	13.966	165	40	49.518	270	49	82.704
55	19	13.966	166	40	49.518	271	50	87.519
56	19	13.966	167	40	49.518	272	50	87.519
57	20	14.884	168	40	49.518	273	50	87.519
58	20	14.884	169	40	49.518	274	50	87.519
59	20	14.884	170	40	49.518	275	50	87.519
60	21	15.85	171	40	49.518	276	50	87.519
61	21	15.85	172	40	49.518	277	50	87.519
62	21	15.85	173	41	52.452	278	50	87.519
57	20	14.884	174	41	52.452	279	50	87.519
58	20	14.884	175	41	52.452	280	50	87.519
59	20	14.884	176	41	52.452	281	50	87.519
60	21	15.85	177	41	52.452	282	50	87.519
61	21	15.85	178	41	52.452	283	50	87.519
62	21	15.85	179	41	52.452	284	50	87.519
63	21	15.85	180	41	52.452	285	51	92.614

(continued)

Table B.2 (continued)

h_S (kJ/kg)	T ($^\circ C$)	x_S (kg/kg)	h_S (kJ/kg)	T ($^\circ C$)	x_S (kg/kg)	h_S (kJ/kg)	T ($^\circ C$)	x_S (kg/kg)
64	22	16.879	181	42	55.45	286	51	92.614
65	22	16.879	182	42	55.45	287	51	92.614
66	22	16.879	183	42	55.45	288	51	92.614
67	22	16.879	184	42	55.45	289	51	92.614
68	23	17.97	185	42	55.45	290	51	92.614
69	23	17.97	186	42	55.45	291	51	92.614
70	23	17.97	187	42	55.45	292	51	92.614
71	23	17.97	188	42	55.45	293	51	92.614
72	24	19.118	189	42	55.45	294	51	92.614
73	24	19.118	190	42	55.45	295	51	92.614
74	24	19.118	191	43	58.816	296	51	92.614
75	24	19.118	192	43	58.816	297	51	92.614
76	25	20.336	193	43	58.816	298	51	92.614
77	25	20.336	194	43	58.816	299	51	92.614
78	25	20.336	195	43	58.816	300	52	98.007
79	25	20.336	186	42	55.45	301	52	98.007
80	26	21.626	187	42	55.45	302	52	98.007
81	26	21.626	186	42	55.45	303	52	98.007
82	26	21.626	187	42	55.45	304	52	98.007
83	26	21.626	188	42	55.45	305	52	98.007
84	27	22.987	189	42	55.45	306	52	98.007
85	27	22.987	190	42	55.45	307	52	98.007
86	27	22.987	191	43	58.816	308	52	98.007
87	27	22.987	192	43	58.816	309	52	98.007
88	27	22.987	193	43	58.816	310	52	98.007
89	28	24.422	194	43	58.816	311	52	98.007
90	28	24.422	195	43	58.816	312	52	98.007
91	28	24.422	196	43	58.816	313	52	98.007
92	28	24.422	197	43	58.816	314	52	98.007
93	29	25.944	198	43	58.816	315	52	98.007
94	29	25.944	199	43	58.816	316	53	103.728
95	29	25.944	200	43	58.816	317	53	103.728
96	29	25.944	201	44	62.261	318	53	103.728
97	29	25.944	202	44	62.261	319	53	103.728
98	29	25.944	203	44	62.261	320	53	103.728
99	30	27.52	204	44	62.261	321	53	103.728
100	30	27.52	205	44	62.261	322	53	103.728
101	30	27.52	206	44	62.261	323	53	103.728